

Observations of Barrier Layer Seasonal Variation in the Banda Sea

M. F. A. Ismail^{1,2} , J. Karstensen¹ , A. Sulaiman², B. Priyono² , A. Budiman², A. Basit², A. Purwandana² , and T. Arifin²

¹GEOMAR Helmholtz Centre for Ocean Research Kiel, Kiel, Germany, ²National Research and Innovation Agency of Indonesia, Jakarta, Indonesia

Key Points:

- First study estimating barrier layer thickness (BLT) in the Banda Sea using comprehensive observations
- A quasi-permanent barrier layer exists in the Banda Sea with seasonal variation in occurrence and thickness
- The intrusion of low saline waters and anticyclonic circulation are identified as the main mechanisms for creating and modulating the local BLT

Supporting Information:

Supporting Information may be found in the online version of this article.

Correspondence to:

M. F. A. Ismail,
fismail@geomar.de

Citation:

Ismail, M. F. A., Karstensen, J., Sulaiman, A., Priyono, B., Budiman, A., Basit, A., et al. (2024). Observations of barrier layer seasonal variation in the Banda Sea.

Journal of Geophysical Research: Oceans, 129, e2023JC020829. <https://doi.org/10.1029/2023JC020829>

Received 15 DEC 2023

Accepted 15 MAY 2024

Author Contributions:

Conceptualization: M. F. A. Ismail

Data curation: B. Priyono, A. Budiman, A. Basit, A. Purwandana, T. Arifin

Formal analysis: M. F. A. Ismail

Funding acquisition: M. F. A. Ismail

Investigation: A. Budiman, A. Basit, A. Purwandana

Methodology: M. F. A. Ismail, J. Karstensen

Project administration: J. Karstensen, A. Sulaiman, T. Arifin

Supervision: J. Karstensen, A. Sulaiman

Visualization: M. F. A. Ismail

Writing – original draft: M. F. A. Ismail

Abstract The Banda Sea is of crucial importance for the circulation of the world's oceans, as it is part of the connection between the Pacific to the Indian Ocean. One peculiarity of the upper ocean hydrography in the Banda Sea is the occurrence of barrier layers. The regionality and temporal variability of barrier layer thickness (BLT) in the Banda Sea are examined in this study utilizing in-situ observations and ocean reanalysis output. It is found that a barrier layer occurs in over 90 % of the observational data profiles, and in over 72 % of those profiles, the BLT is shallower than 10 m. Furthermore, we find a seasonal cycle in BLT with a maximum thickness of about 60 m occurring during austral autumn and winter and coinciding with the presence of low saline waters fed by the regional river discharge and rainfall from the Java Sea and Makassar Strait. In addition, we identify the existence of a quasi-permanent anticyclonic circulation cell in the Banda Sea that may support the trapping of surface freshwater by retention. The anticyclonic circulation is most likely wind-driven because it coincides with the regional Ekman pumping pattern. Modulation of the anticyclone is via seasonal variability in the wind stress curl which in turn may explain the efficiency of freshwater retention and thus the BLT. The annual mean BLT distribution in the Banda Sea shows a preferential region of thickened barrier layers around 6°-8°S and 124°-126°E and resampling the pattern of the monthly mean climatology.

Plain Language Summary The Banda Sea is crucial to the circulation of the world's oceans and atmosphere due to its location within the equatorial regions of the Indonesian Maritime Continent. It links the Pacific and Indian Oceans' circulation via the Indonesian Throughflow and contributes to driving atmospheric conditions via heat and moisture fluxes. Strong salinity-stratified barrier layers insulate the water exchange between the surface and subsurface. The formation and seasonal variation of barrier layer thickness (BLT) in the Banda Sea are analyzed based on all available observations and ocean reanalysis outputs. Observations show that the Banda Sea has a barrier layer for the most part of the season. The BLT maximum appears during austral winter (June to August) months. The seasonal BLT maximum is attributed to the near-surface water freshening, which shoals the mixed layer depth (MLD) and deep isothermal layer depth (ILD) maintained by a steady anticyclonic gyre. Other processes, such as wind stress curl-induced Ekman pumping associated convergence, also modulate its seasonal variability.

1. Introduction

A surface mixed layer with vertically quasi-homogenous properties in temperature and salinity exists over a large part of the global ocean (de Boyer Montégut et al., 2004). A region with a strong density gradient, the pycnocline, generally marks the base of the mixed layer. Air-sea interactions permanently modify mixed layer properties, and the downward propagation of properties from the air/sea interface is due to a complex interaction of buoyancy (composed of heat and freshwater forcing) and momentum fluxes mediated by mixing processes. In tropical oceans, the seasonality of heat flux is less pronounced compared to the subtropical or the high latitude ocean. However, one phenomenon that is well developed over parts of the tropical ocean is the formation of barrier layers (Lukas & Lindstrom, 1991; Sprintall & Tomczak, 1992). A freshwater surplus at the ocean surface, either from rainfall or riverine sources, can create its own, and sometimes very local, density gradient within an otherwise rather homogenous in temperature (and density) layer. This way the low salinity-driven mixed layer depth (MLD) can be shallower than a temperature-defined isothermal layer depth (ILD) that characterizes more the background mixed layer. A layer difference between the MLD and deeper ILD is referred to as the barrier layer because it acts as a barrier against the vertical exchange of heat, salt, and momentum between the near-surface and the top of the thermocline (Drushka et al., 2014; Kara et al., 2003; Katsura et al., 2022). Lukas and Lindstrom (1991) were the

© 2024. The Author(s).

This is an open access article under the terms of the [Creative Commons Attribution License](https://creativecommons.org/licenses/by/4.0/), which permits use, distribution and reproduction in any medium, provided the original work is properly cited.

Writing – review & editing:
M. F. A. Ismail, J. Karstensen

first to study the barrier layer in the Western Equatorial Pacific and found it linked to local buoyancy gain of the ocean surface by heavy precipitation. Barrier layers have attracted increasing research interest and have been documented globally (de Boyer Montégut et al., 2007) in many regional oceans, such as in the Arabian Sea (e.g., Thadathil et al., 2008), the Bay of Bengal (e.g., Kumari et al., 2018), the Indo-Australian Basin (e.g., Qu & Meyers, 2005), and the South China Sea (e.g., Liang et al., 2018).

The development of barrier layers involves various physical mechanisms that regulate the ILD and MLD, including wind-driven downwelling (e.g., Pang et al., 2019), horizontal advection of low salinity waters (e.g., George et al., 2019), net freshwater fluxes (e.g., Katsura et al., 2022), and relative vorticity (e.g., d'Ovidio et al., 2013). It is suggested that barrier layer thickness (BLT) extends from several meters to a hundred meters and varies temporally and spatially (de Boyer Montégut et al., 2007; Mignot et al., 2007). The existence of barrier layers has substantial thermodynamic and dynamic implications. It is found that barrier layers in tropical oceans limit the upward intrusion of cold thermocline water into the mixed layer, trap heat in the mixed layer, and lessen the impacts of atmospheric heat forcing on the mixed layer (Drushka et al., 2014; Katsura et al., 2022). Both processes enhance regional surface temperature anomalies and elevate atmospheric convection (Ivanova et al., 2021; Li et al., 2017). The evolution of BLT influences air-sea exchange on time scales ranging from sub-seasonal (Pujiana & McPhaden, 2018) to seasonal time scales (Felton et al., 2014). Early research has shown the barrier layer's impact on large-scale ocean-atmosphere interactions in the Indian Ocean (Drushka et al., 2014; Kumari et al., 2018) and the Pacific Ocean (Corbett et al., 2017; Maes et al., 2005). Using an observational and coupled ocean-atmosphere model, Maes et al. (2005) demonstrated the significant role of barrier layers in maintaining anomalous warm water over the equatorial eastern Pacific, ultimately promoting the formation of El Niño Southern Oscillation. In the Indian Ocean, Qiu et al. (2012) highlighted a robust link between barrier layer variability and the formation of the Indian Ocean Dipole. Further, they suggested that an Indian Ocean Dipole - induced co-varying barrier layer improves the Indian Ocean Dipole positive feedback. A recent study by Ivanova et al. (2021) has shown that the variability of BLT in the East Indian Ocean strongly correlates with the rainfall over West Sumatra and Australia. Further, Ivanova et al. (2021) argued that barrier layers might be used to predict intensified rainfall over northern Australia. The preceding studies highlight the significant role of barrier layers in controlling ocean-atmosphere interactions, which impact weather and climate.

The Banda Sea (Figure 1a) is the largest tropical semi-enclosed sea in the Indonesian Maritime Continent. Due to its unique location, the Banda Sea is essential to the circulation of the world's oceans and atmosphere (Gordon et al., 1994; Lee et al., 2019; Wang et al., 2023; Yin et al., 2023; Yoneyama & Zhang, 2020; Yuan et al., 2022). It connects the tropical Pacific and Indian Oceans' circulation via the Indonesian Throughflow and contributes to regional climate through heat, salt, and momentum fluxes (Atmadipoera et al., 2022; Jochum & Potemra, 2008; Yin et al., 2023; Yuan et al., 2022). At intraseasonal time scales, the Banda Sea surface temperature is modulated by the Madden-Julian Oscillation (Napitu et al., 2015; Pei et al., 2021). The upper ocean circulation in the Banda Sea is controlled by seasonally reversing monsoonal winds from the northwest during the austral summer and from the southeast during the austral winter (Gordon & Susanto, 2001; Ilahude & Gordon, 1996; Ismail et al., 2023; Kida et al., 2019; Sprintall & Liu, 2005; Zhu et al., 2019). The southeast monsoon drives basin-wide wind-induced mixing (Thomas et al., 2003), strong outflow through the Timor Passage and into the Indian Ocean (Kida et al., 2019), and quasi-stationary anticyclonic eddy in the southwest boundary of the Banda Sea (Liang et al., 2019; Zhu et al., 2019). In contrast, the northwest monsoon current carries low salinity water from the Java Sea and Makassar Strait through rainfall and river discharge (Halkides et al., 2011; Ilahude & Gordon, 1996; Kida et al., 2019; Zhu et al., 2019). This freshwater influx, which has a pronounced low sea surface salinity signature (<34), is overlying saline subsurface water and creates a strong salinity stratification in the Banda Sea that is forming a regional barrier layer (Ismail et al., 2023).

Barrier layers in the eastern Indian Ocean and west of the Indonesian Maritime Continent have been suggested to warm the upper ocean and in turn intensify the rainfall in Australia and Indonesia (Ivanova et al., 2021). So far, little attention has been given to the drivers and variability of the barrier layer in the Banda Sea. Ismail et al. (2023) used data from a single Argo float from the eastern Banda Sea to document the temporal evolution of salinity stratification and barrier layer thickness. Here, we extend the earlier study and examine the spatial distribution and variation of barrier layers in the Banda Sea. We also consider the physical processes that support and maintain their formation and bridge this information with the local climate forcing. We make use of all available historical observations data from multiple platforms (i.e., conductivity-temperature-salinity-depth (CTD) instruments and Argo floats) and also consider data from an ocean reanalysis model.

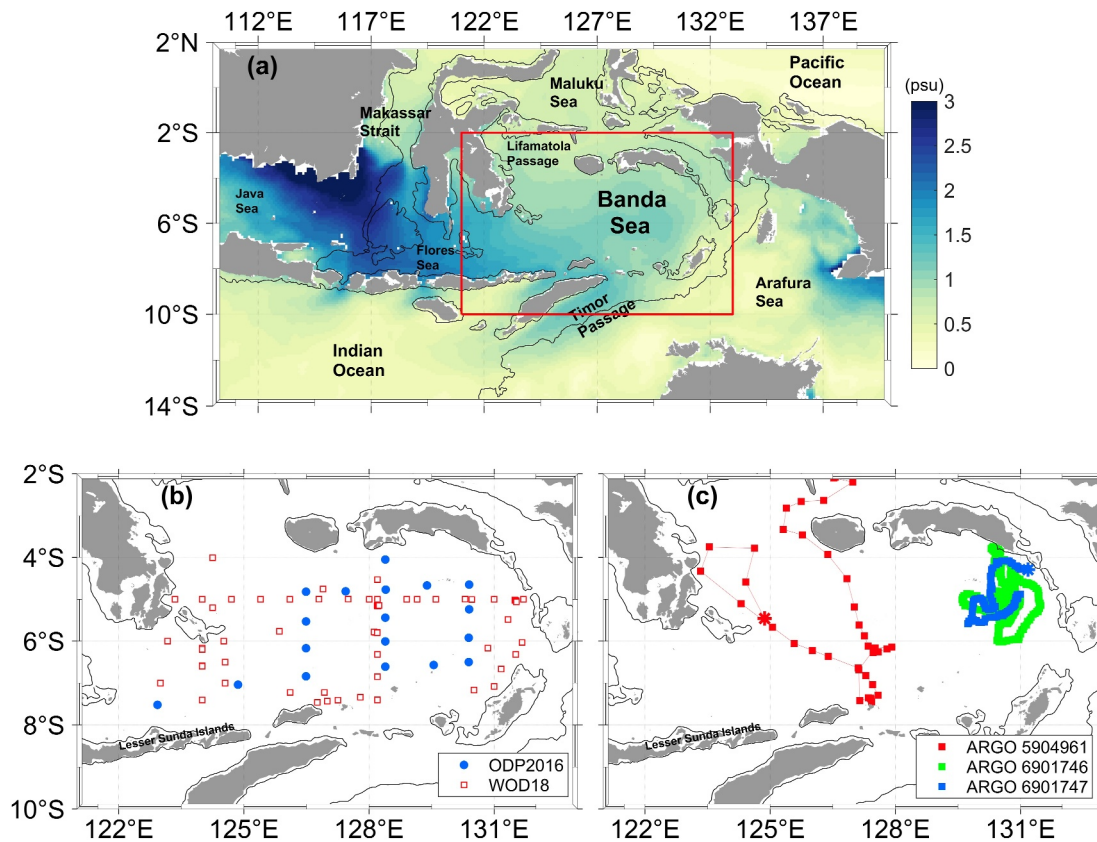


Figure 1. (a) Geographic features of the Indonesian Seas overlaid with the magnitude of the seasonal cycle in salinity from January 1993–December 2022 based on the Bluelink ReANalysis version 2020. (b) Positions of CTD stations of the Ocean Dynamics Program for the Banda Sea and stations archived in the World Ocean Database 2018. (c) CTD profile positions (squares) and trajectories (lines) of Argo floats 5904961, 6901746, and 6901747. The red rectangle in (a) outlined the location of the area captured in (b) and (c). The red, green, and blue asterisk in (c) denotes the end location of Argo floats 5904961, 6901746, and 6901747, respectively. The solid black lines in a, b, and c denote the 500 m isobath.

2. Materials and Methods

2.1. Observational Data

The historical CTD data used in this study originates from the Ocean Dynamics Program for the Banda Sea (ODP2016) and several research field campaigns archived in the World Ocean Database 2018 (WOD18) and include the International Oceanographic Data and Information Exchange project and NOAA National Center for Environmental Information (Boyer et al., 2018). The ODP2016 cruise (Figure 1b) consisted of 18 CTD profiles (upper 1,000 m) of temperature and salinity measured using the SBE 911+ system onboard the *RV Baruna Jaya VIII* between 29 August and 5 September 2016 (Table 1). The WOD18 data consists of 80 CTD profiles collected between 1993 and 2001 (Figure 1b and Table 1). CTD data from three Argo floats (ID: 5904961, 6901746, and 6901747) are also used (Figure 1c).

2.2. Ocean and Atmosphere Reanalysis Products

The gridded data from the Bluelink ReANalysis version 2020 (BRAN2020) model is used to investigate the BLT seasonal climatology from January 1993 to December 2022 and to add to the individual CTD station's observational data a coherent time/space context. BRAN2020 is based on the global eddy-resolving Ocean Forecasting Australia Model released in May 2021 (Chamberlain et al., 2021; Oke et al., 2013; Schiller et al., 2020). A complete description of Ocean Forecasting Australia Model is provided by Oke et al. (2013). The model has 1/12° horizontal resolution for all longitudes, between latitude 75°S to 75°N, and 51 vertical levels with 5 m vertical resolution down to 40 m, 10 m vertical resolution from 40 to 200 m, and 500 m thick below 2,000 m. BRAN2020 outputs realistically produce the ocean circulation and perform comparatively well compared to Argo floats

Table 1
General Statistics of the Observed Barrier Layer in the Banda Sea

Source	Observation periods	Number of profiles	% Occurrence of BLT >2 m	Mean BLT (m)
ODP2016	29 August 2016–5 September 2016	18	94.44	9.05
WOD18	29 July 1992–4 August 1992	10	90.00	11.57
	29 August 1993–3 September 1993	15	93.33	8.50
	31 January 1994–09 February 1994	17	94.12	7.91
	12 November 1995–13 November 1995	5	100.00	2.30
	04 December 1996–13 December 1996	17	94.12	4.12
	28 February 1998–4 March 1998	16	100.00	13.57
Argo 5904961	23 June 2018–8 December 2018	31	97.77	13.42
Argo 6901746	29 July 2017–28 August 2019	414	90.09	9.17
Argo 6901747	4 September 2018–7 April 2019	109	89.91	9.67

observations in the Banda Sea (Figure S1 to S3 in Supporting Information S1). It shall be noted that Argo float data we use for our analysis is also assimilated in the BRAN2020. A recently published study evaluating three global ocean reanalysis products demonstrates that BRAN2020 outperforms the Hybrid Coordinate Ocean Model and Mercator Ocean's Global Reanalysis in Southern Africa, especially for the MLD (Russo et al., 2022). Numerous researches in the Australasian region have been supported by BRAN2020 data, including analysis of the Fraser Gyre off southeast Queensland (Ismail et al., 2017), studies of intraseasonal variability of the Indonesian Throughflow (Schiller et al., 2010), and mixed layer heat and mass budget in the Banda Sea (Ismail et al., 2023). Near-surface zonal and meridional wind data for the period January 1993 to December 2022 from the fifth generation of the global climate and weather outputs of the European Center for Medium-Range Weather Forecasts (Hersbach et al., 2023) were also used in this study.

2.3. Determining ILD, MLD, BLT, and Relative Vorticity

The ILD and MLD are computed according to the de Boyer Montégut et al. (2004) and Holte and Talley (2009) algorithms. The ILD is computed as the interpolated depth where the temperature ($^{\circ}\text{C}$) has decreased by 0.2°C from the reference depth of 10 m. The reference depth of 10 m is utilized to eliminate the diurnal variations of ocean surface water at the first few meters (Breugem et al., 2008). The MLD is computed as the interpolated depth at which potential density (σ_{θ}) increases from the reference depth (10 m) by the equivalent value of 0.03 kg m^{-3} . The BLT is the positive difference between the ILD and MLD with at least 2 m in magnitude.

From BRAN2020, we compute the relative vorticity ζ (s^{-1}) to characterize the ocean's local rotational flow (Rudnick et al., 2019) and as an indicator of mesoscale processes that may be linked to the distribution of BLT in the Banda Sea. The relative vorticity is computed as follows:

$$\zeta = \frac{\partial v}{\partial x} - \frac{\partial u}{\partial y} \quad (1)$$

Where u and v are zonal and meridional velocity (m s^{-1}) from BRAN2020, and x and y are zonal and meridional position. Positive and negative relative vorticity represent anticyclonic and cyclonic mesoscale features.

3. Results and Discussion

3.1. Evidence of the Barrier Layer From Observations

As example, Figure 2 show selected temperature, salinity, and density profiles over the upper 200-m from ODP2016 and Argo 5904961 in the Banda Sea. The respective ILD, MLD, and BLT are indicated. For both profiles, the halocline aligns well with the pycnocline. Moreover, the upper thermocline layers that mark the ILD are about 50 m (80 m) deep in ODP2016 (Argo 5904961), with large vertical fluctuation between the 14 and 28°C isotherms. While temperature tends to be nearly homogenous from the surface to the upper thermocline layer, salinity increases from approximately 34.15 to 34.40 (33.90–34.20) from about 20 to 40 m (20–80 m) depth

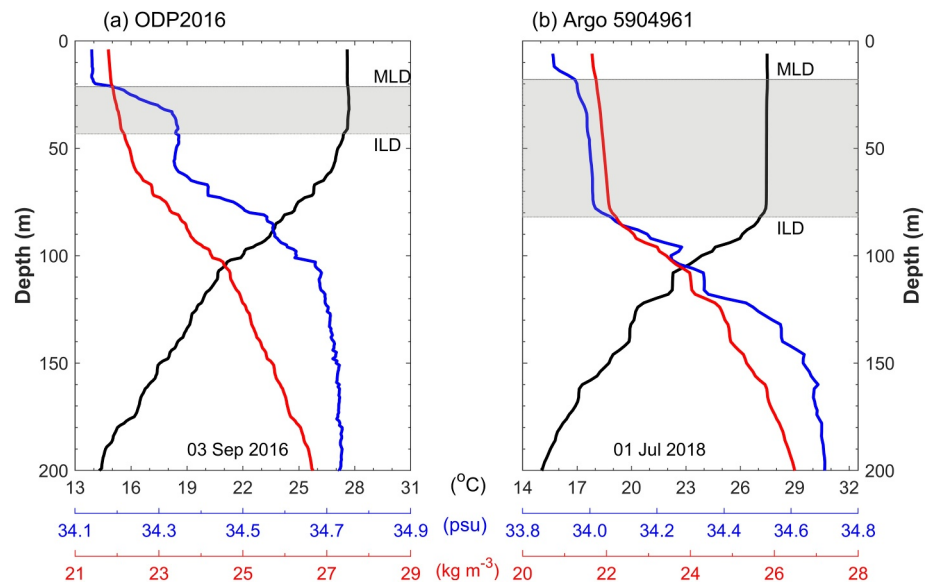


Figure 2. Vertical profiles of temperature ($^{\circ}\text{C}$; black line), salinity (psu ; blue line), and density (kg m^{-3} ; red line) in the Banda Sea from (a) ODP2016 on 3 September 2016, and (b) Argo 5904961 on 1 July 2018. The gray lines denote the MLD, and the dashed gray lines represent the ILD. The gray-shaded area is the section of the water column termed BLT.

(Figure 2). This salinity increase causes a shallow density gradient near a depth of about 20 m and inside the ILD. Figures 2a and 2b also reveal that pycnoclines in the Banda Sea are likely determined by salinity. A halocline above the thermocline leads to the MLD becoming shallower than the ILD, indicating the existence of a barrier layer. The MLD on 03 September 2016 is about 20 m. Below it is a barrier layer about 21 m thick (Figure 2a). Similar shallower MLD was also observed on 01 July 2018, albeit the barrier layer is thicker, exceeding 60 m (Figure 2b).

The barrier layer occurrence distributions have been observed for more than 90% of all profiles (Table 1) in the Banda Sea. For example, among 18 CTD stations during the ODP2016 cruise, there are 17 stations where the barrier layer occurs. Thus, the rate of occurrence reaches 94.44%, though most of the BLT is under 9 m Table 1 shows two groups of CTD data with high occurrence rates of BLT in the Banda Sea. They were observed from 12–13 November 1995 and 28 February to 4 March 1998. These BLT have a mean value ranging from 2.30 to 13.57 m (see Table 1). To explore the spatial distribution of BLT in the Banda Sea, we computed all observation profiles and projected them into a geographical map (Figure 3a). The results denote that BLT is generally shallow, with about 72% of profiles having BLT less than 10 m. BLT deeper than 30 m are predominantly obtained from Argo profiles along its trajectories. To further analyze BLT distribution from all observations, we computed the probability density function (Figure 3b). It appears that high BLT densities are in the range of 2–10 m, which is in line with BLT spatial distribution (Figure 3a). In addition, the probability density function is highly skewed toward an increase of BLT values.

To assess the seasonal variation of BLT from observations in the Banda Sea, we quantified the statistical values of the BLT in each season shown in Figure 3c. The available data acquired during different seasons and years allow us to estimate a seasonal cycle that is, December to February (DJF) represents austral summer, March to May (MAM) illustrates austral autumn, June to August (JJA) defines austral winter, and September to November (SON) represents austral spring. The analysis shows that the barrier layer was found to be thicker in MAM and JJA than in SON and DJF. The seasonality of BLT was highly significant, with p values < 0.001 . The thick barrier layer during MAM (JJA) exhibited a median value of 8.0 m (6.0 m) with upper quartiles above 13 m depth. The maximum value of BLT during MAM and JJA reached 66 and 64 m, respectively. Those maximum values were obtained from Argo 6901746 and Argo 5904961, respectively. In contrast, thin barrier layers are found in SON. The median of BLT during DJF and SON is 6 and 4 m, respectively, with both upper quartiles below 13 m. During DJF (SON), it is observed that the highest value of BLT reaches at most 52 m (30 m). The statistical analysis

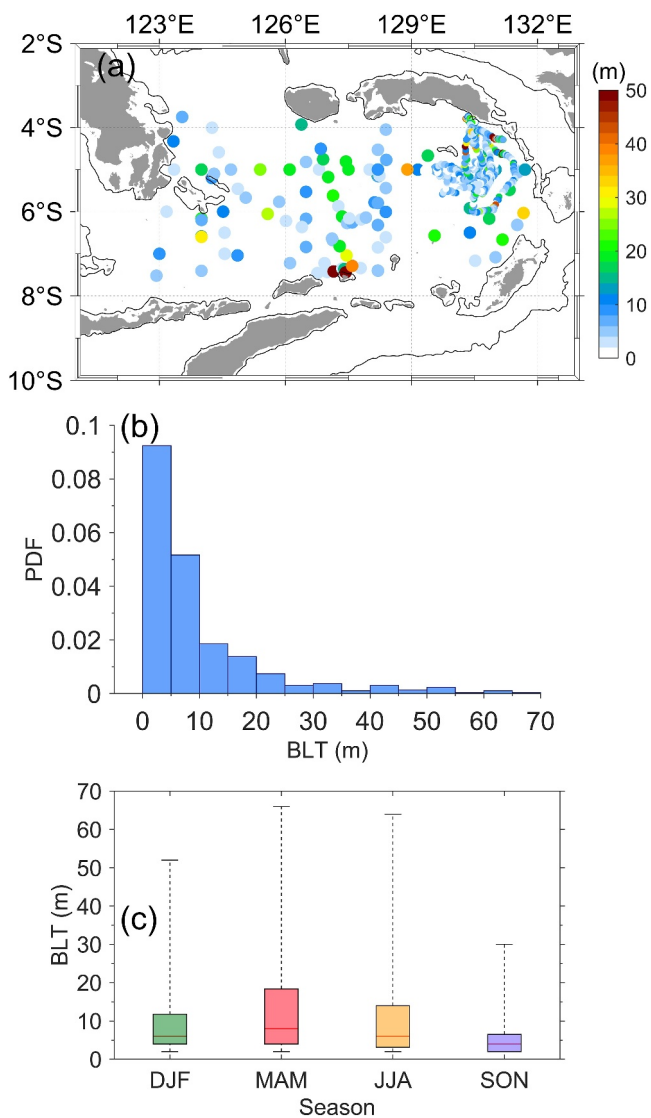


Figure 3. (a) Spatial distribution, (b) probability density distribution (%), and (c) box-whisker plots of BLT (m) estimated from all observations in the Banda Sea. The boxes in (c) are defined by lower and upper quartiles, and the center red lines in the boxes represent the median, caps at the end of the boxes exhibit minimum and maximum values. The solid black lines in (a) show the 500 m isobaths.

above suggests that the estimated BLT from observations in the Banda Sea has an apparent seasonal variation, with BLT maximum and minimum observed in MAM and SON, respectively.

The source of the upper layer water masses entering the Banda is identified using potential temperature-salinity diagrams (Figure 4). The potential temperature-salinity diagrams showed that fresher (<34) and relatively warm ($>27^{\circ}\text{C}$) water masses within σ_{θ} values range of $20\text{--}22\text{ kg m}^{-3}$ observed almost in all season in the Banda Sea, except during the SON. Previous studies identified this surface water as Java Surface Water (JSW). JSW is characterized by a homogenous salinity below 34, potential temperature between $27\text{--}30^{\circ}\text{C}$, and σ_{θ} values below 22.00 kg m^{-3} (Atmadipoera et al., 2022; Ilahude & Gordon, 1996; Kida et al., 2019). Kida et al. (2019) demonstrated that the source of the JSW is intense net precipitation during DJF in the Java Sea. In the Banda Sea, JSW first appeared during DJF (Figure 4a) and reached its peak occurrence during MAM (Figure 4b). During JJA the JSW presence declines (Figure 4c) while during SON it is not observed in the Banda Sea (Figure 4d). The presence of JSW in the Banda Sea during DJF, MAM, and JJA indicated direct intrusion of the regional river discharge and rainfall from the Java Sea and Makassar Strait (see Figure 1a). Through applying a particle tracking model, Kida et al. (2019) suggested that the JSW remains and accumulates near the surface of the Banda Sea from December to May before exiting through the Timor Passage between October and November. The existence of JSW in the Banda Sea caused a decrease in salinity, which later induced a shallower MLD compared to ILD, thus thickening the barrier layer in the Banda Sea.

The time series of the barrier layer derived from temperature and salinity profiles from all available three Argo floats in the Banda Sea is shown in Figure 5. In general, the vertical temperature in the upper 150 m shows seasonal temperature increases, reaching above 29°C from December to April, after which it decreases to below 26°C from June to August (Figure 5a–5c). The seasonal buildup of near-surface warm (cold) waters during DJF (JJA) is a distinct feature of the Banda Sea (Gordon & Susanto, 2001; Ismail et al., 2023). The 29°C (26°C) isotherm during January–February (July–August) extends to about 100 m (70 m) depth, which marks the base of the ILD. Below the ILD, the thermocline exists in which the temperature reduces significantly by 15°C over a depth range of about 100 m. The thermocline layer average position exhibits significant upward and downward movement on seasonal time scales in phase with the ILD. The first maxima of the thermocline layer occur mainly in February–March, and the second maxima in July–August. Like the thermocline variability, the ILD from Argo 6901746 (eastern Banda Sea) shows seasonal variability with a bimodal distribution.

The first maxima of about 90–100 m deep, was observed in February/March, and the second maxima reached up to 70 m deep during July–August (Figure 5a). Because both cover only one season, Argo 5904961 and 6901747 were captured only one peak of deeper ILD (Figures 5b and 5c). Following Argo 6901746, the ILD maximum from Argo 5904961 (6901747) also appeared in July–August (February–March), reaching up to 80 m.

Like the temperature, the time-depth salinity profiles show seasonal variations in the upper 100 m depth (Figure 5). The salinity structures of the upper layers during the observational period of Argo float 6901746, covering roughly two years, also show two freshening events (Figure 5), while Argo floats 5904961 and 6901747 both show only one freshening event, due to their shorter (less than a year) deployment time, but well synchronized with Argo 6901746. The freshening events are characterized by relatively low saline water ranging from 32.0 to 34.0 in the upper 70 m, mainly observed from February to June. Moreover, for Argo 6901746 the near-surface fresh layer tends to last longer in 2018 compared to 2019. The maximum near-surface salinity above 34.5 appears between September and November. During the freshening periods, two waters with contrasting

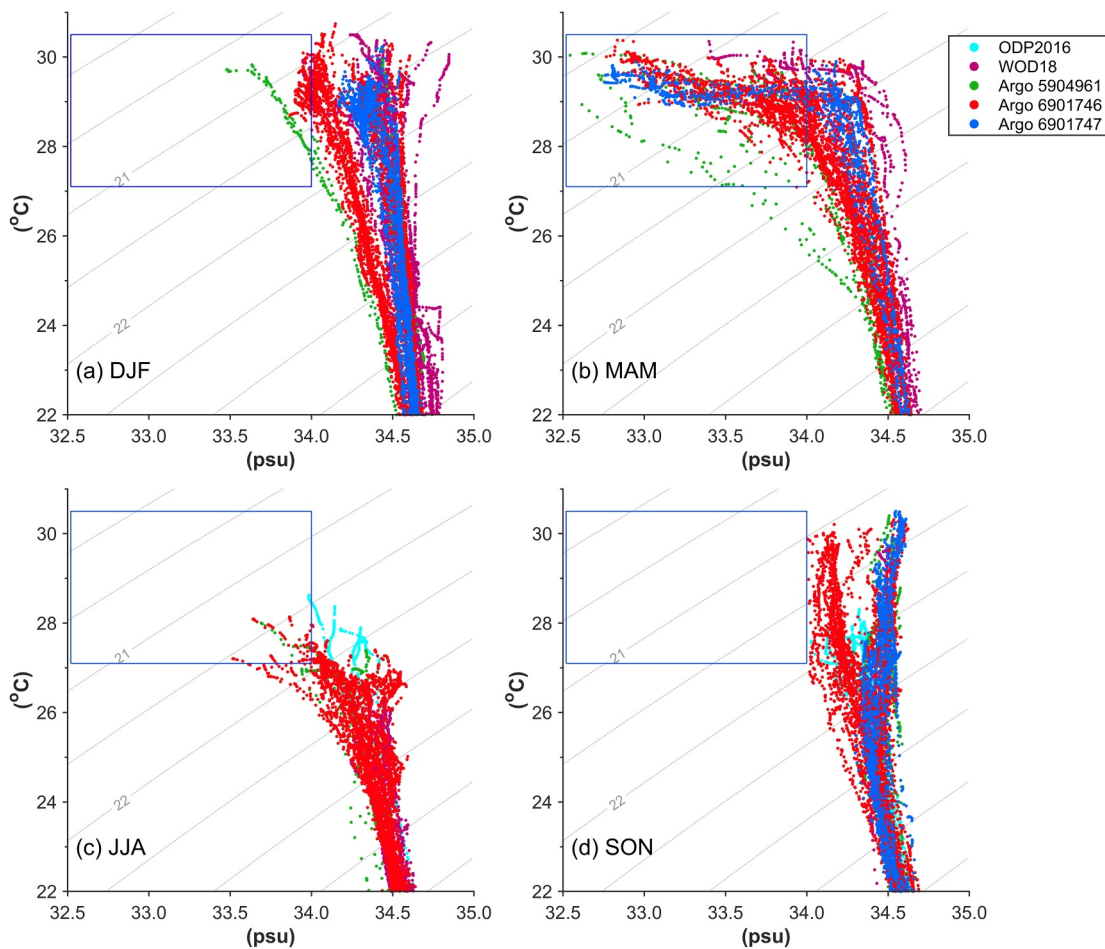


Figure 4. Potential temperature ($^{\circ}\text{C}$) versus salinity diagram in the upper ocean layer for (a) December to February (DJF), (b) March to May (MAM), (c) June to August (JJA), and (d) September to November (SON) obtained from all observations in the Banda Sea (Figures 1b and 1c). The gray contours with numbers show isopycnic lines. The blue rectangle indicates the characteristics of JSW.

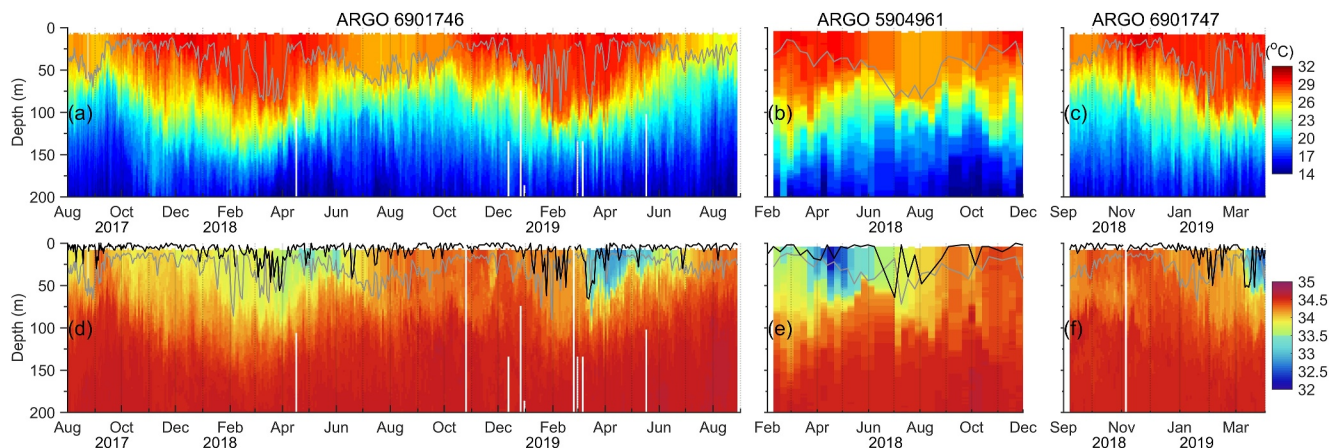


Figure 5. Time series of upper 200 m of (a, b, c) temperature ($^{\circ}\text{C}$) and (d, e, f) salinity in the Banda Sea from Argo 6901746 (left panel), Argo 5904961 (middle panel), and Argo 6901747 (right panel). Gray lines in (a, b, c, d, e, f) show the ILLD (MLD), while black lines in d, e, f represent the BLT.

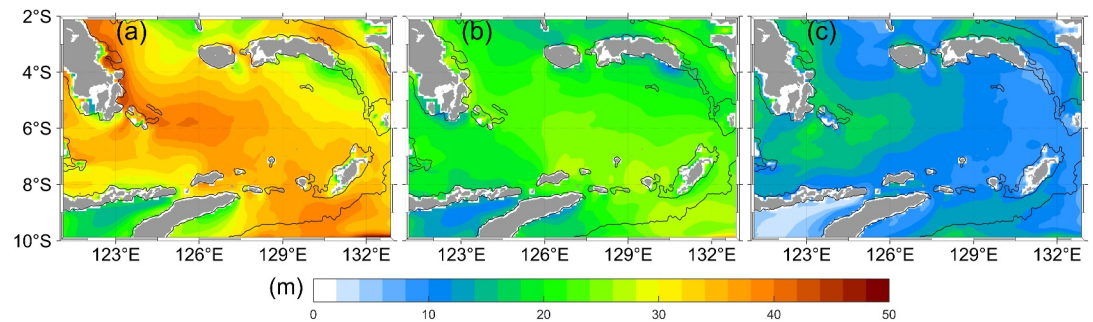


Figure 6. Climatological annual mean of (a) ILL, (b) MLD, and (c) BLT from 1993 to 2022. Black lines in (a, b, and c) represent the 500 m isobath. The ILL, MLD, and BLT are computed from the gridded product of BRAN2020 data sets.

salinities in the vertical are becoming visible. The separation is between the near-surface low-salinity water and subsurface high-salinity water that sits below 70 m depth, indicating a strong salinity stratification in the Banda Sea that coincides with a relatively shallow MLD (>25 m). It shall be noted that a shoaling of the MLD is also visible during the salinization events in SON. The upper-layer freshening is suspected to be linked to the eastward advection of JSW into the Banda Sea. Further, seasonal temperature and salinity profiles from Argo floats reveal that the ILL is almost always deeper than the MLD, indicating the appearance of seasonal barrier layers.

The BLT from Argo 6901746 shows seasonality with a bimodal distribution (Figure 5d). The barrier layer reaches the first maxima of more than 60 m depth in February–April. It attains the second maxima (<40 m) in June–July. However, the thickened barrier layer in February–April is highly variable and sporadic, which appears to be linked to the local rainfall pattern in the eastern Banda Sea. A recent study by Ismail et al. (2023) shows that there is increased atmospheric convection from February to April, corresponding with a significant rise in precipitation. The thickened barrier layer in June–July is more of a classical deepening picture with less variability in time series. Because of the shorter time series (roughly one year), the BLT from Argo 5904961 and 6901747 only show one peak in June–July (Figure 5e) and March–April (Figure 5f), respectively and this synchronized with Argo 6901746 2-year record. It is worth noting that the thick barrier layer reaches about 64 m in June–July, only captured by Argo 5904961 circling in the central/western Banda Sea (Figure 1c), suggesting that the barrier layer occurs in the western-central Banda Sea. The strong signal that originates from the JSW advection is not fully captured by Argo 6901746 operating in the eastern Banda Sea, and thus the BLT maximum in June–August is limited in vertical extent. Similarly, Argo 6901747’s operating for about 8–9 months and covering only during September to May. The BLT maximum in June–August mainly reflects that of the ILL (Figures 5a and 5b). Less than 10 m of barrier layer were observed from Argo 5904961 and 6901746 found during September–November in 2018 and 2019. Overall, the occurrence rates of barrier layer (>2 m) have been identified for almost all profiles of Argo 5904961, with a mean value of 13.42 m. The occurrence rates of BLT from Argo 6901746 and Argo 6901747 are about 90% (Table 1), and have a mean thickness value ranging from 9.17 to 9.67 m.

3.2. Barrier Layer Mean Conditions

In order to set the variability into a context, we derived mean conditions of ILL, MLD, and BLT (Figures 6 and 7) from the BRAN2020 reanalysis product. The mean ILL distribution (Figure 6a) is deeper than 30 m over a large part of the Banda Sea. A band of maximum ILL core with values close to 50 m is found in the midwest of the Banda Sea, extending from the 5° to 7°S latitude and 125° to 128°E longitude, as well as north-westward along the west boundary of Lifamatola Passage. The mean MLD distribution is mainly shallower than the ILL and ranges from about 16 to 28 m (Figure 6b). The spatial patterns of ILL and MLD exhibit significant differences in value. The shallower MLD and deeper ILL indicate the presence of thick barrier layers, as demonstrated in Figure 6c. The mean BLT spatial structure clearly shows a band of BLT deeper than 20 m observed along a path similar to the ILL maximum. The BLT maximum appears to be located in the western region of the Banda Sea and centered around 5°–7°S and 124°–126°E. In contrast, BLT shallower than 10 m is mainly contained east of the Banda Sea. The annual mean analysis provides a preferential region of the thicker barrier layers in the Banda Sea.

The monthly evolution of BLT (Figure 7) exhibits seasonal variation with distinct spatial structures. Spatial characteristics of BLT distribution deeper than 10 m are generally along the northern half of the Banda Sea

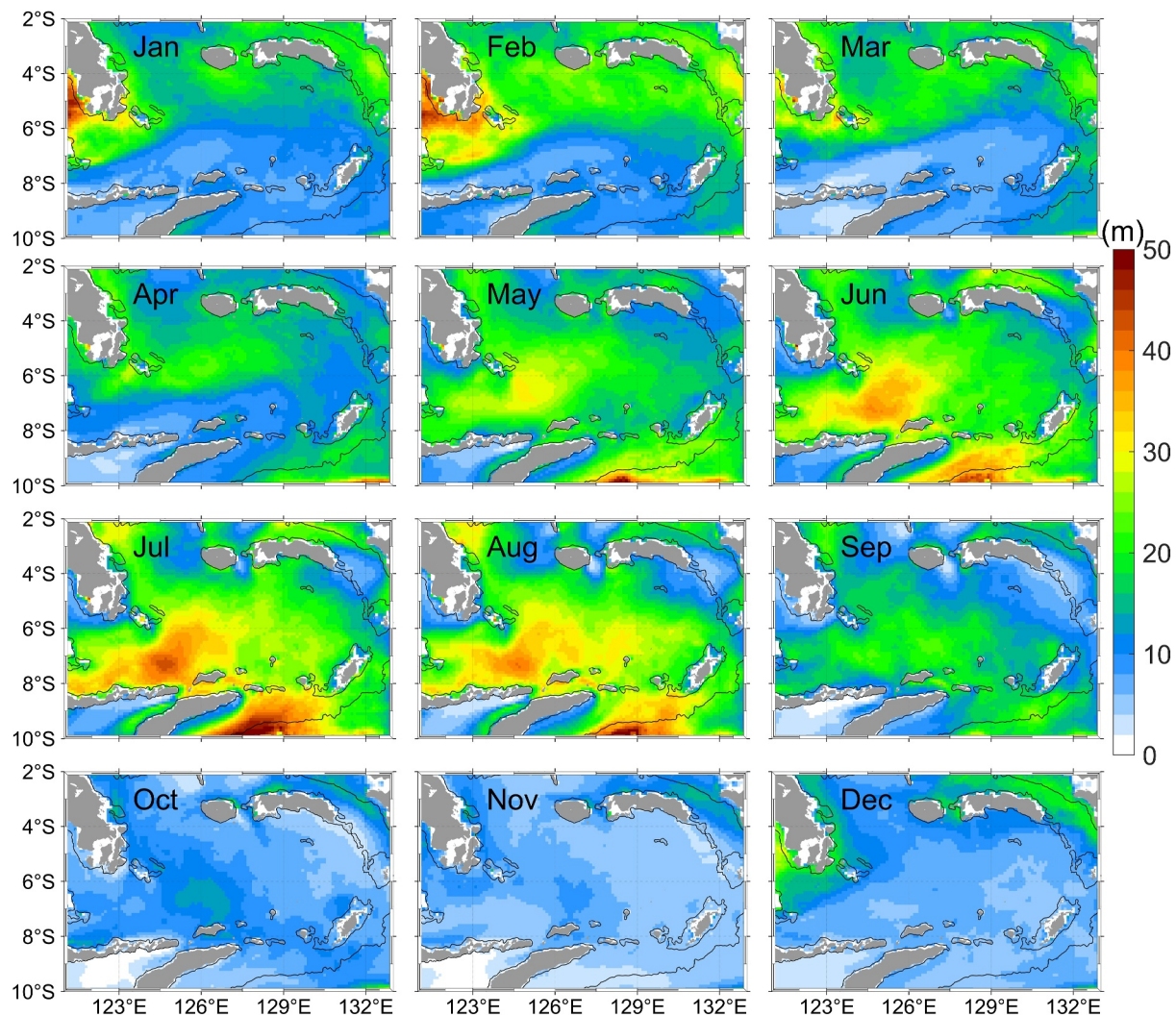


Figure 7. Monthly mean BLT (m) climatology in the Banda Sea based on BRAN2020 data from January 1993 to December 2022. Solid black lines represent the 500 m isobath.

between February and March/April. In addition, a band of shallower BLT (<10 m) is observed along the southern half of the Banda Sea. By May, the region of barrier layers formed in the northern half of the Banda Sea builds up both in thickness and spatial extent southward.

During the JJA, the spatial distribution of BLT displays a noticeably different pattern from that of the DJF and MAM. The thick barrier layers (>20 m) covered almost the entire Banda Sea during this period. It is observed that the BLT attains its seasonal maximum in JJA and is over 40 m deep in the mid-west of the Banda Sea, which is consistent with the BLT maximum observed with Argo 5904961 (Figure 5e). This region of high BLT appears as a rather steady feature that has not been reported in the past. The region that encompasses the seasonal BLT maximum during JJA in Figure 7 agrees with the pattern of the annual mean structure shown in Figure 6c. This similarity suggests a significant contribution of BLT during the JJA to the annual mean field. With the beginning of the SON, the barrier layers undergo a weakening phase. Its spatial extent begins to decrease by September, albeit thick BLT (~20 m) still occurs in a large area spanning from the center to the west of the Banda Sea (Figure 7). In October and November, the BLT mainly decreases to under 10 m with the thick barrier layers core centered around 6°S to 8°S latitude and 124°E and 126°E longitude. The weakest BLT is observed in November and December, with its value generally not more than 10 m, and appears in a thin and patchy in the Banda Sea. The BLT formation can be summarized into four major stages: the initial stage during DJF, the development and peak stages in MAM and JJA, respectively, and the decaying stage in SON.

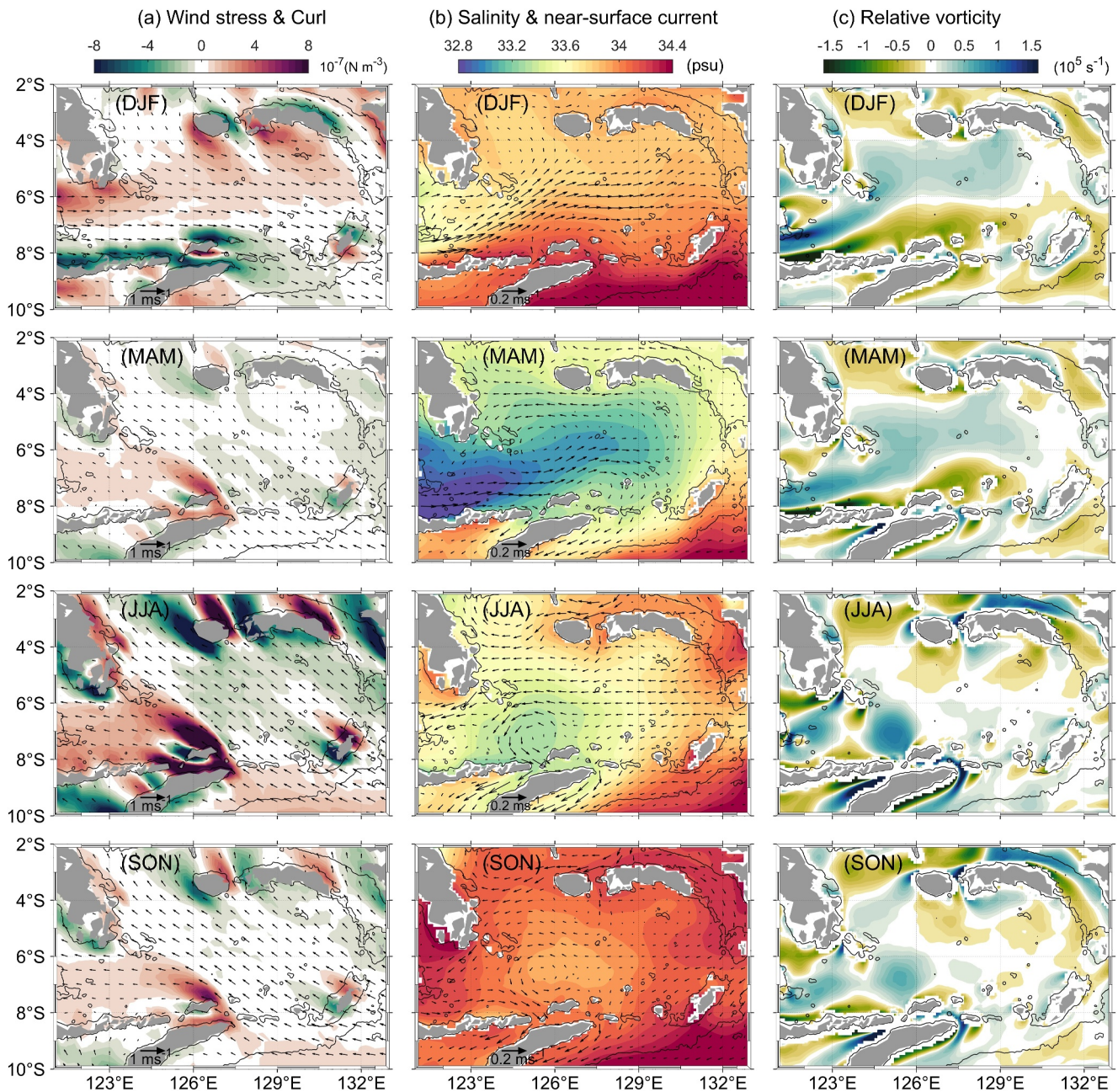


Figure 8. Seasonal monthly climatology of (a) wind stress (vectors) overlaid with wind stress curl (10^{-7} N m^{-3}), (b) surface salinity overlaid with near-surface current (vectors) from BRAN2020, and (c) relative vorticity (10^5 s^{-1}) during the period of January 1993 to December 2022 in the Banda Sea. The black contour lines represent the 500 m isobath. Wind stress and wind stress curl are computed using the fifth generation of the global climate and weather outputs of the European Center for Medium-Range Weather Forecasts winds. Relative vorticity is calculated from BRAN2020.

3.3. Possible Mechanism of the Seasonal BLT Variation

To understand the drivers of the seasonal BLT variation in the Banda Sea, we analyzed wind stress and wind stress curl, horizontal salinity advection, and mesoscale relative vorticity as a proxy for mesoscale activity. During DJF, the wind stress is northwesterly in the northern region of the Banda Sea and westerly in the south (Figure 8a). Simultaneously, the surface circulation is in general northeast over the entire Banda Sea with the strongest current in the southwestern and central parts and weakest currents in the north (Figure 8a). Westerly winds during the austral summer monsoon season create a positive curl north of about 7°S and a very strong negative curl at the southern boundary of the domain. From the north-eastward flow, a branch separates into eastward and northward

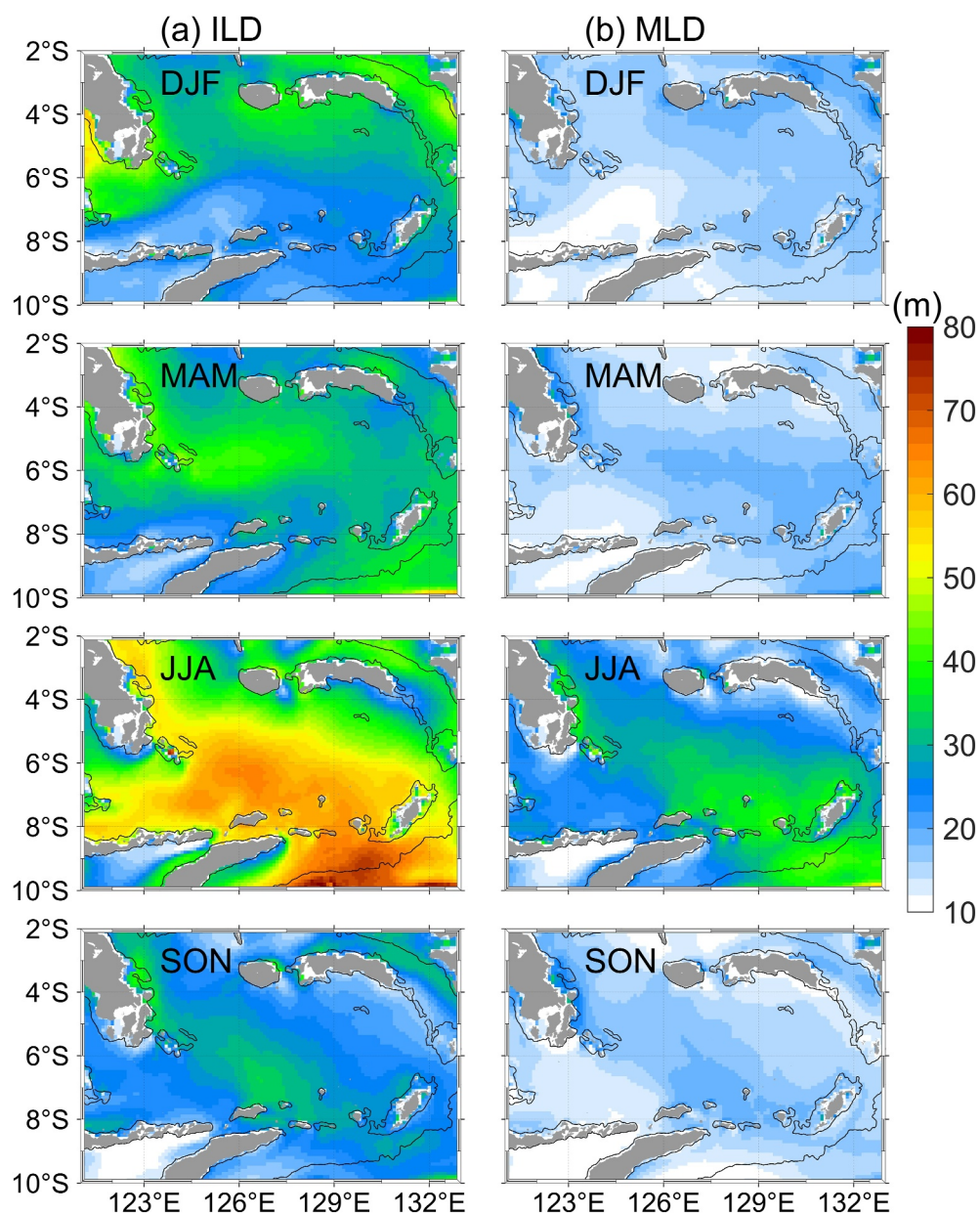


Figure 9. Seasonal monthly climatology of (a) ILD (m) and (b) MLD (m) for the period of January 1993 to December 2022 in the Banda Sea. The 500 m isobaths are shown in black lines. ILD and MLD are calculated from BRAN2020.

flows at around 126°E longitude (Figure 8b). From a surface salinity point of view, the eastward flow can bring JSW into the Banda Sea. It is also responsible for the positive and negative relative vorticity due to the zonal shear in the flow field (Figure 8c). The positive and negative relative vorticity establishes a near-surface double gyre circulation in the basin: an anticyclonic circulation in the northern and cyclonic circulation in the southern part of the Banda Sea that observed during DJF. A recent modeling study by Zhu et al. (2019) also reported this particular circulation pattern. In line with anticyclonic circulation in the northern half of the Banda Sea, a warm sea surface temperature (Figure 5) and an ILD deepening (Figure 9a) are found. Meanwhile, the eastward advection of low salinity water from the Java Sea supports a shoaling of the MLD (Figure 9b). The difference between them begins to emerge, leading to a distinct BLT distribution in the north and the south of the Banda Sea (see Figure 7).

The spatial distribution of thicker BLT expands during the onset of southeasterly winds in MAM, consistent with the evolution of the ILD. The BLT deepening during this period is likely regulated by the freshening of the upper

water column due to the further redistribution of JSW and supported by anticyclonic circulation. These can be manifested in the spatial distribution of the thickened BLT core (Figure 7) that emulates freshening salinity events and widening positive relative vorticity, as shown in Figures 8b and 8c. In addition, the deepened ILD (Figure 9a) concurred with the dominated positive relative vorticity region (Figure 8c). The presence of an anticyclonic circulation pattern during MAM likely corresponded with longer water retention, which influenced the ocean's upper layer dynamic (d'Ovidio et al., 2013) and contributed to the ILD deepening. The relatively weak south-easterly wind stress during monsoon transition drives a sluggish southwestward Ekman transport and slight wind-driven mixing (Halkides et al., 2011; Sprintall & Liu, 2005; Thomas et al., 2003) that could lead to the slight deepening of ILD and MLD. However, the presence of the low salinity of JSW over the high salinity water during MAM generates strong salinity stratification, which shoals the MLD that are relatively similar to those of DJF (Figure 9b). This freshwater of JSW is trapped over the Banda Sea and spreads along the Timor Passage toward the eastern Indian Ocean (Kida et al., 2019), which can be seen in Figure 8b. The significant role of low salinity water horizontal advection to the MLD was also observed by Halkides et al. (2011) and Ismail et al. (2023). The resultant ILD thickening and MLD shoaling then favor a deep barrier layer in the Banda Sea forced by a shallow MLD that limits the momentum input to the near-surface mixed layer only. Consistent with the zonal band of deep ILD, the thickened barrier layer occurs during MAM. Further, the filament of a thick barrier layer (>20 m) always appears in the low salinity region and positive relative vorticity distribution in the Banda Sea (Figures 8b and 8c).

The physical mechanisms that lead to the peak phase of the BLT in the Banda Sea during JJA are explored. The thickened BLT distribution in JJA likely corresponds with the convergence of the Ekman transport estimated from the wind stress curl and robust positive relative vorticity, particularly on the central and western Banda Sea and low salinity water of JSW over the central basin (Kida et al., 2019). A very good coincidence exists between the BLT maximum (~50 m), as shown during JJA in Figure 7, with positive wind stress curl, relatively low salinity water, and intense positive relative vorticity indicative of anticyclonic circulation cell centered in the 7°S latitude and 125°E longitude (Figure 8). A possible explanation is that the Ekman transport convergence that supports the anticyclonic circulation cell also generates deeper ILD and MLD (see Figure 9). During this time, the energetic wind stress curls induce Ekman downwelling (upwelling) primarily on the western (eastern) side of the Banda Sea (Gordon & Susanto, 2001; Thomas et al., 2003). While we expect that upwelling favors ILD and MLD shallowing and vice versa, an early study by Gordon and Susanto (2001) in the Banda Sea during JJA suggested that upwelling favorable wind was always associated with cooler near-surface temperature but not always with shallower ILD. Using a mixed layer heat and salinity budget, Halkides et al. (2011) argued that a strong southeast monsoon increases wind-driven vertical diffusivity that causes ILD and MLD to deepen. However, Thomas et al. (2003) hypothesized that the shallowing ILD and MLD are eroded by the intense southeasterly wind-induced mixing, which also contributes to the ILD and MLD deepening (Figure 9). Although both ILD and MLD are deepening, ILD is always deeper than MLD, therefore dominating the thickening of barrier layers spatial pattern in the Banda Sea during JJA.

The decaying phase of BLT in the Banda Sea during SON is in line with the changes in wind stress from southeasterly winds and an associated relaxation in the curl Ekman pumping, respectively. More saline waters appear at the surface, and also the surface ocean is affected by a net evaporation changing of salinity regime to salinization-dominated waters (Halkides et al., 2011; Ismail et al., 2023) and a remnant of positive relative vorticity in the same spot as in JJA. The characteristics of ILD and MLD spatial distribution are slightly similar to those of during MAM, except that their thickness is shallower. The presence of higher salinity surface water over the Banda Sea leads to weak stratification and a thick MLD. However, Halkides et al. (2011) suggested that the wind stress curl from the southeasterly winds will shoal the pycnocline, thus against the MLD deepening due to weak stratification. At the same time, the vertical temperature shows a weaker gradient than the vertical salinity due to higher net heat gain by the ocean, which favors a thickened ILD than MLD (Halkides et al., 2011; Ismail et al., 2023). The thickened barrier layer (~10m) during SON is restricted to the western side of the Banda Sea. It distributes symmetrically with the positive relative vorticity, suggesting the role of an anticyclonic gyre in maintaining deep ILD and modulating the BLT spatial distribution during SON.

4. Summary and Conclusions

The seasonal evolution of the Barrier Layer occurrence in the Banda Sea and the potential drivers for the seasonality have been analyzed. This way, we extend the study by Ismail et al. (2023), based on a single Argo float in

the eastern Banda Sea, to the whole area. We use all the available in-situ CTD profile data and also consider ocean reanalysis model data BRAN2020. In the CTD data, barrier layers are identified for more than 90% of profiles, with about 72% with a thickness of less than 10 m. We also found a quasi-permanent barrier layer exists in the Banda Sea but with seasonal variations. The BLT maximum and minimum in the Banda Sea were identified in June–August and September–November, respectively. Observations also displayed that thickened barrier layers in the Banda Sea concurred with the freshening events between February and July. We have shown that these freshening events were caused by the eastward advection of low salinity JSW near the surface, which created a MLD shoaling.

The annual climatological mean distribution of BLT in BRAN2020 illustrated a hot spot of thicker barrier layers in the central/western region of the Banda Sea and centered around 6° – 8° S and 124° – 126° E. This pattern also is evident in the monthly mean fields. Our results suggest that the monthly climatological cycle of BLT can be divided into four stages according to its seasonal variation: the initial stage during DJF, the development and peak stage in MAM and JJA, respectively, and the attenuation stage in SON. In its initial stage, the barrier layer forms when Ekman pumping and anticyclonic circulation increase and in turn deepen the ILD. On the contrary, the advection of low salinity surface water from the Java Sea shoals the MLD. The development period of BLT in MAM is mainly attributed to the near-surface water freshening due to the presence of JSW that induces strong vertical salinity stratification, which shoals the MLD and deep ILD maintained by enhanced anticyclonic gyre. The freshening events during MAM provide a precondition for the development of shallower MLD in the following months. The combination of energetic southeasterly wind, anticyclonic circulation cells, and relatively low salinity water from JSW are more pronounced for the peak period of BLT in JJA. The convergence zone due to wind stress curl-induced Ekman pumping and robust anticyclonic circulation cells favor a deep ILD and MLD, albeit MLD deepening is limited by salinity stratification. We found that strong southeasterly wind stress in JJA also contributes to deepening the ILD and MLD through wind-driven mixing and vertical, upward mixing of higher salinity subsurface water, as previously documented by Halkides et al. (2011) and Thomas et al. (2003). During SON, the barrier layers are the thinnest of the year. Though their thickness is shallower, the ILD and MLD spatial distributions are marginally comparable to those during the MAM. The BLT is likely maintained by the southeasterly wind stress and curl corresponding with shoaled the pycnocline and MLD and relatively thickened ILD related to the higher net heat gain by the ocean as noted in Halkides et al. (2011) and Ismail et al. (2023).

Here, we provide a first description of the BLT seasonal cycle and identify the processes that control the seasonal barrier layer's development and erosion in the Banda Sea. We demonstrated the presence of a quasi-permanent anticyclonic circulation cell in the Banda Sea, which might facilitate the retention of low-salinity surface water during MAM and JJA and thus help to maintain a thick BLT and a shallow MLD, respectively. Given that the anticyclonic circulation aligns with the regional Ekman pumping pattern, it is most likely driven by wind. Modulation of the anticyclonic gyre is via seasonal variability in the wind stress curl, which may explain the efficiency of freshwater retention. It thus helps maintain the BLT and make it more coherent during JJA. The mechanisms responsible for the BLT variation discussed here can be applied to subtropical and equatorial regions where mesoscale circulation patterns and substantial freshwater influx are prevalent. The BLT has a notable impact on the sea surface temperature.

This study's description of BLT and its seasonal variation may help understand the ocean's role in air-sea interaction processes regulating substantial sea surface temperature cooling in the Banda Sea (Pei et al., 2021). It is worth emphasizing that the thickening of barrier layers off west Sumatra relates to increased rainfall over northern Australia (Ivanova et al., 2021). We will explore this potential link of the thermal impact of the barrier layer in the Banda Sea to the local rainfall over the Indonesian Maritime Continent in the future. The analysis presented in this work focuses mainly on the BLT's seasonal change and annual mean state. It also is a study that shows that the BRAN2020 provides a very good state description for the Banda Sea region. However, it is known that intraseasonal and interannual oceanic and atmospheric variability in the Banda Sea is significant, arising from tropical atmospheric phenomena such as Madden-Julian Oscillation (Napitu et al., 2015) and large-scale climate of the Indo-Pacific region, including the Indian Ocean Dipole (Yoneyama & Zhang, 2020) and El Niño Southern Oscillation (Gordon & Susanto, 2001). In future work, we will investigate the quantitative analysis of the remote forcing mechanisms driving BLT variability at intraseasonal and interannual time scales.

Data Availability Statement

Argo data were compiled and made freely available by the International Argo Program and the national programs contributing to it (<http://www.argo.ucsd.edu>, <http://argo.jcommops.org>). The Argo Program is part of the Global Ocean Observing System of the Coriolis Data Assembly Center (<http://doi.org/10.17882/42182>). The ODP2016 data, documentation, and information are available at <https://zenodo.org/records/11180802>. WOD18 data, documentation, and information can be found at <http://www.nodc.noaa.gov/OC5/indprod.html>. The BRAN2020 data are available at <https://doi.org/10.25914/6009627c7af03>. ERA5 data provided by the Copernicus Climate Change Service (C3S) Climate Data Store can be found at <https://doi.org/10.24381/cds.adbb2d47>.

Acknowledgments

This work is funded by the Georg Foster Research Fellowship of the Alexander von Humboldt-Stiftung. MFAI acknowledges support from GEOMAR Helmholtz Centre for Ocean Research Kiel and the National Research and Innovation Agency of Indonesia (BRIN). The authors thank three anonymous reviewers for their constructive comments and suggestions. Open Access funding enabled and organized by Projekt DEAL.

References

- Atmadipoera, A. S., Koch-Larrouy, A., Madec, G., Grelet, J., Baurand, F., Jaya, I., & Dadou, I. (2022). Part I: Hydrological properties within the eastern Indonesian throughflow region during the INDOMIX experiment. *Deep Sea Research Part I: Oceanographic Research Papers*, *182*, 103735. <https://doi.org/10.1016/j.dsr.2022.103735>
- Boyer, T., Baranova, O., Coleman, C., Garcia, H., Grodsky, A., Locarnini, R., et al. (2018). World Ocean Database 2018. NOAA Atlas NESDIS 87. Mishonov, Technical Ed.
- Breugem, W.-P., Chang, P., Jang, C., Mignot, J., & Hazeleger, W. (2008). Barrier layers and tropical Atlantic SST biases in coupled GCMs. *Tellus A: Dynamic Meteorology and Oceanography*, *60*(5), 885–897. <https://doi.org/10.3402/tellusa.v60i5.15505>
- Chamberlain, M. A., Oke, P. R., Fiedler, R. A., Beggs, H. M., Brassington, G. B., & Divakaran, P. (2021). Next generation of Bluelink ocean reanalysis with multiscale data assimilation: BRAN2020. *Earth System Science Data*, *13*(12), 5663–5688. <https://doi.org/10.5194/essd-13-5663-2021>
- Corbett, C. M., Subrahmanyam, B., & Giese, B. S. (2017). A comparison of sea surface salinity in the equatorial Pacific Ocean during the 1997–1998, 2012–2013, and 2014–2015 ENSO events. *Climate Dynamics*, *49*(9), 3513–3526. <https://doi.org/10.1007/s00382-017-3527-y>
- de Boyer Montégut, C., Madec, G., Fischer, A. S., Lazar, A., & Iudicone, D. (2004). Mixed layer depth over the global ocean: An examination of profile data and a profile-based climatology. *Journal of Geophysical Research*, *109*(C12). <https://doi.org/10.1029/2004jc002378>
- de Boyer Montégut, C., Mignot, J., Lazar, A., & Cravatte, S. (2007). Control of salinity on the mixed layer depth in the World Ocean: 1. General description. *Journal of Geophysical Research*, *112*(C6). <https://doi.org/10.1029/2006jc003953>
- d’Ovidio, F., De Monte, S., Della Penna, A., Cotté, C., & Guinet, C. (2013). Ecological implications of eddy retention in the open ocean: A Lagrangian approach. *Journal of Physics A: Mathematical and Theoretical*, *46*(25), 254023. <https://doi.org/10.1088/1751-8113/46/25/254023>
- Drushka, K., Sprintall, J., & Gille, S. T. (2014). Subseasonal variations in salinity and barrier-layer thickness in the eastern equatorial Indian Ocean. *Journal of Geophysical Research: Oceans*, *119*(2), 805–823. <https://doi.org/10.1002/2013jc009422>
- Felton, C. S., Subrahmanyam, B., Murty, V. S. N., & Shriver, J. F. (2014). Estimation of the barrier layer thickness in the Indian Ocean using Aquarius Salinity. *Journal of Geophysical Research: Oceans*, *119*(7), 4200–4213. <https://doi.org/10.1002/2013jc009759>
- George, J. V., Vinayachandran, P. N., Vijith, V., Thushara, V., Nayak, A. A., Pargaonkar, S. M., et al. (2019). Mechanisms of barrier layer formation and erosion from in situ observations in the Bay of Bengal. *Journal of Physical Oceanography*, *49*(5), 1183–1200. <https://doi.org/10.1175/jpo-d-18-0204.1>
- Gordon, A. L., Ffield, A., & Ilahude, A. G. (1994). Thermocline of the Flores and Banda seas. *Journal of Geophysical Research*, *99*(C9), 18235–18242. <https://doi.org/10.1029/94jc01434>
- Gordon, A. L., & Susanto, R. D. (2001). Banda Sea surface-layer divergence. *Ocean Dynamics*, *52*(1), 2–10. <https://doi.org/10.1007/s10236-001-8172-6>
- Halkides, D., Lee, T., & Kida, S. (2011). Mechanisms controlling the seasonal mixed-layer temperature and salinity of the Indonesian seas. *Ocean Dynamics*, *61*(4), 481–495. <https://doi.org/10.1007/s10236-010-0374-3>
- Hersbach, H., Bell, B., Berrisford, P., Biavati, G., Horányi, A., Muñoz Sabater, J., et al. (2023). ERA5 hourly data on single levels from 1979 to present. *Copernicus Climate Change Service (C3S) Climate Data Store (CDS)*.
- Holte, J., & Talley, L. (2009). A new algorithm for finding mixed layer depths with applications to Argo data and Subantarctic Mode Water formation. *Journal of Atmospheric and Oceanic Technology*, *26*(9), 1920–1939. <https://doi.org/10.1175/2009jtecho543.1>
- Ilahude, A. G., & Gordon, A. L. (1996). Thermocline stratification within the Indonesian seas. *Journal of Geophysical Research*, *101*(C5), 12401–12409. <https://doi.org/10.1029/95jc03798>
- Ismail, M. F. A., Karstensen, J., Ribbe, J., Arifin, T., Chandra, H., Akhwyd, R., et al. (2023). Seasonal mixed layer temperature and salt balances in the Banda Sea observed by an Argo float. *Geoscience Letters*, *10*(1), 1–9. <https://doi.org/10.1186/s40562-023-00266-x>
- Ismail, M. F. A., Ribbe, J., Karstensen, J., Lemckert, C., Lee, S., & Gustafson, J. (2017). The Fraser Gyre: A cyclonic eddy off the coast of eastern Australia. *Estuarine, Coastal and Shelf Science*, *192*, 72–85. <https://doi.org/10.1016/j.ecss.2017.04.031>
- Ivanova, D. P., McClean, J. L., Sprintall, J., & Chen, R. (2021). The oceanic barrier layer in the eastern Indian Ocean as a predictor for rainfall over Indonesia and Australia. *Geophysical Research Letters*, *48*(22), e2021GL094519. <https://doi.org/10.1029/2021gl094519>
- Jochum, M., & Potemra, J. (2008). Sensitivity of tropical rainfall to Banda Sea diffusivity in the Community climate system model. *Journal of Climate*, *21*(23), 6445–6454. <https://doi.org/10.1175/2008jcli2230.1>
- Kara, A. B., Rochford, P. A., & Hurlburt, H. E. (2003). Mixed layer depth variability over the global ocean. *Journal of Geophysical Research*, *108*(C3). <https://doi.org/10.1029/2000jc000736>
- Katsura, S., Sprintall, J., Farrar, J. T., Zhang, D., & Cronin, M. F. (2022). The barrier layer effect on the heat and freshwater balance from Moored observations in the eastern Pacific fresh Pool. *Journal of Physical Oceanography*, *52*(8), 1705–1730. <https://doi.org/10.1175/jpo-d-21-0243.1>
- Kida, S., Richards, K. J., & Sasaki, H. (2019). The fate of surface freshwater entering the Indonesian seas. *Journal of Geophysical Research: Oceans*, *124*(5), 3228–3245. <https://doi.org/10.1029/2018jc014707>
- Kumari, A., Kumar, S. P., & Chakraborty, A. (2018). Seasonal and interannual variability in the barrier layer of the Bay of Bengal. *Journal of Geophysical Research: Oceans*, *123*(2), 1001–1015. <https://doi.org/10.1002/2017jc013213>
- Lee, T., Fournier, S., Gordon, A. L., & Sprintall, J. (2019). Maritime Continent water cycle regulates low-latitude chokepoint of global ocean circulation. *Nature Communications*, *10*(1), 2103. <https://doi.org/10.1038/s41467-019-10109-z>

- Li, Y., Han, W., Wang, W., Ravichandran, M., Lee, T., & Shinoda, T. (2017). Bay of Bengal salinity stratification and Indian summer monsoon intraseasonal oscillation: 2. Impact on SST and convection. *Journal of Geophysical Research: Oceans*, *122*(5), 4312–4328. <https://doi.org/10.1002/2017jc012692>
- Liang, L., Xue, H., & Shu, Y. (2019). The Indonesian throughflow and the circulation in the Banda Sea: A modeling study. *Journal of Geophysical Research: Oceans*, *124*(5), 3089–3106. <https://doi.org/10.1029/2018jc014926>
- Liang, Z., Xie, Q., Zeng, L., & Wang, D. (2018). Role of wind forcing and eddy activity in the intraseasonal variability of the barrier layer in the South China Sea. *Ocean Dynamics*, *68*(3), 363–375. <https://doi.org/10.1007/s10236-018-1137-9>
- Lukas, R., & Lindstrom, E. (1991). The mixed layer of the western equatorial Pacific Ocean. *Journal of Geophysical Research*, *96*(S01), 3343–3357. <https://doi.org/10.1029/90jc01951>
- Maes, C., Picaut, J., & Belamari, S. (2005). Importance of the salinity barrier layer for the buildup of El Niño. *Journal of Climate*, *18*(1), 104–118. <https://doi.org/10.1175/jcli-3214.1>
- Mignot, J., de Boyer Montégut, C., Lazar, A., & Cravatte, S. (2007). Control of salinity on the mixed layer depth in the World Ocean: 2. Tropical areas. *Journal of Geophysical Research*, *112*(C10). <https://doi.org/10.1029/2006jc003954>
- Napitu, A. M., Gordon, A. L., & Pujiana, K. (2015). Intraseasonal Sea surface temperature variability across the Indonesian seas. *Journal of Climate*, *28*(22), 8710–8727. <https://doi.org/10.1175/jcli-d-14-00758.1>
- Oke, P. R., Griffinn, D. A., Schiller, A., Matear, R., Fiedler, R., Mansbridge, J., et al. (2013). Evaluation of a near-global eddy-resolving ocean model. *Geoscientific Model Development*, *6*(3), 591–615. <https://doi.org/10.5194/gmd-6-591-2013>
- Pang, S., Wang, X., Liu, H., Zhou, G., & Fan, K. (2019). Decadal variability of the barrier layer and forcing mechanism in the Bay of Bengal. *Journal of Geophysical Research: Oceans*, *124*(7), 5289–5307. <https://doi.org/10.1029/2018jc014918>
- Pei, S., Shinoda, T., Steffen, J., & Seo, H. (2021). Substantial Sea surface temperature cooling in the Banda Sea associated with the Madden-Julian oscillation in the Boreal winter of 2015. *Journal of Geophysical Research: Oceans*, *126*(6), e2021JC017226. <https://doi.org/10.1029/2021JC017226>
- Pujiana, K., & McPhaden, M. J. (2018). Ocean surface layer response to convectively coupled Kelvin waves in the eastern equatorial Indian Ocean. *Journal of Geophysical Research: Oceans*, *123*(8), 5727–5741. <https://doi.org/10.1029/2018jc013858>
- Qiu, Y., Cai, W., Li, L., & Guo, X. (2012). Argo profiles variability of barrier layer in the tropical Indian Ocean and its relationship with the Indian Ocean Dipole. *Geophysical Research Letters*, *39*(8). <https://doi.org/10.1029/2012gl051441>
- Qu, T., & Meyers, G. (2005). Seasonal variation of barrier layer in the southeastern tropical Indian Ocean. *Journal of Geophysical Research*, *110*(C11). <https://doi.org/10.1029/2004jc002816>
- Rudnick, D. L., Zeiden, K. L., Ou, C. Y., Johnston, T. S., MacKinnon, J. A., Alford, M. H., & Voet, G. (2019). Understanding vorticity. *Oceanography*, *32*(4), 66–73. <https://doi.org/10.5670/oceanog.2019.412>
- Russo, C. S., Veitch, J., Carr, M., Fearon, G., & Whittle, C. (2022). An intercomparison of global reanalysis products for Southern Africa’s major oceanographic features. *Frontiers in Marine Science*, *9*, 284. <https://doi.org/10.3389/fmars.2022.837906>
- Schiller, A., Brassington, G. B., Oke, P., Cahill, M., Divakaran, P., Entel, M., et al. (2020). Bluelink ocean forecasting Australia: 15 years of operational ocean service delivery with societal, economic and environmental benefits. *Journal of Operational Oceanography*, *13*(1), 1–18. <https://doi.org/10.1080/1755876x.2019.1685834>
- Schiller, A., Wijffels, S., Sprintall, J., Molcard, R., & Oke, P. R. (2010). Pathways of intraseasonal variability in the Indonesian Throughflow region. *Dynamics of Atmospheres and Oceans*, *50*(2), 174–200. <https://doi.org/10.1016/j.dynatmoce.2010.02.003>
- Sprintall, J., & Liu, W. T. (2005). Ekman mass and heat transport. *Oceanography*, *18*(4), 88–97. <https://doi.org/10.5670/oceanog.2005.09>
- Sprintall, J., & Tomczak, M. (1992). Evidence of the barrier layer in the surface layer of the tropics. *Journal of Geophysical Research*, *97*(C5), 7305–7316. <https://doi.org/10.1029/92jc00407>
- Thadathil, P., Thoppil, P., Rao, R. R., Muraliedharan, P. M., Somayajulu, Y. K., Gopalakrishna, V. V., et al. (2008). Seasonal variability of the observed barrier layer in the Arabian Sea. *Journal of Physical Oceanography*, *38*(3), 624–638. <https://doi.org/10.1175/2007jpo3798.1>
- ThomasMarra, M. J., John, M., & Ali, A. (2003). Response of the Banda Sea to the southeast monsoon. *Marine Ecology Progress Series*, *261*, 41–49. <https://doi.org/10.3354/meps261041>
- Wang, Z., Yin, X., Li, X., Li, Y., Li, R., Yang, Y., et al. (2023). Water mass variations in the Maluku channel of the Indonesian seas during the winter of 2018–2019. *Journal of Geophysical Research: Oceans*, *128*(3), e2022JC018731. <https://doi.org/10.1029/2022jc018731>
- Yin, X., Yuan, D., Li, X., Wang, Z., Li, Y., Corvianawatie, C., et al. (2023). Moored observations of the currents and transports of the Maluku sea. *Journal of Physical Oceanography*, *53*(1), 3–18. <https://doi.org/10.1175/jpo-d-22-0027.1>
- Yoneyama, K., & Zhang, C. (2020). Years of the Maritime Continent. *Geophysical Research Letters*, *47*(12), e2020GL087182. <https://doi.org/10.1029/2020gl087182>
- Yuan, D., Yin, X., Li, X., Corvianawatie, C., Wang, Z., Li, Y., et al. (2022). A Maluku Sea intermediate western boundary current connecting Pacific Ocean circulation to the Indonesian Throughflow. *Nature Communications*, *13*(1), 2093. <https://doi.org/10.1038/s41467-022-29617-6>
- Zhu, Y., Wang, L., Wang, Y., Xu, T., Li, S., Cao, G., et al. (2019). Stratified circulation in the Banda Sea and its causal mechanism. *Journal of Geophysical Research: Oceans*, *124*(10), 7030–7045. <https://doi.org/10.1029/2019jc015279>